

# Topological design of multi-cell hexagonal tubes under axial and lateral loading cases using a modified particle swarm algorithm



Na Qiu<sup>a,b</sup>, Yunkai Gao<sup>a,\*</sup>, Jianguang Fang<sup>c,\*</sup>, Guangyong Sun<sup>d</sup>, Nam H. Kim<sup>b</sup>

<sup>a</sup> School of Automotive Studies, Tongji University, Shanghai 201804, China

<sup>b</sup> Dept. of Mechanical & Aerospace Engineering, University of Florida, Gainesville, FL 32611, USA

<sup>c</sup> Centre for Built Infrastructure Research, School of Civil and Environmental Engineering, University of Technology Sydney, NSW 2007, Australia

<sup>d</sup> School of Aerospace, Mechanical and Mechatronic Engineering, The University of Sydney, Sydney, NSW 2006, Australia

## ARTICLE INFO

### Article history:

Received 4 February 2017

Revised 30 June 2017

Accepted 23 August 2017

Available online 19 September 2017

### Keywords:

Multi-cell hexagonal tube

Topology optimization

Impact

Crashworthiness

Lateral bending

Axial compression

## ABSTRACT

Multi-cell structures have widely been studied due to their excellent energy absorption ability. However, few systematic studies have been conducted on the topological design of cross-sectional configurations of thin-walled tubes. To make full use of the material, topology optimization of multi-cell hexagonal tubes was conducted under both axial compression and lateral bending loadings. A binary particle swarm optimization (PSO) was enhanced by introducing the mass constraint factor to guide the movement of particles, which could improve the success rate of obtaining the global optimum. It was found that the optimum designs under the axial load placed the material outward to strengthen the interaction between the outer and inner walls and created more partitions between the inside rib walls. While under the lateral load, all the optimum designs have diagonally-connected elements to resist local deformation, and the material was also placed outward to increase the moment of inertia and thus to resist the global deformation. For the multiple loading cases, the final optimal designs are similar to the compression designs or combined designs from the two loading cases.

© 2017 Elsevier Inc. All rights reserved.

## 1. Introduction

Recently, structural crashworthiness, which is closely correlated to occupant fatalities, has drawn public attention due to a high customers expectation and rigorous regulation [1–3]. For this reason, thin-walled structures, such as multi-cell columns have been used as energy absorbers to dissipate the kinetic energy when a crash occurs. Considerable studies have been performed to investigate the crashworthiness of multi-cell tubes [4–8]. For example, Kim [9] compared new multi-cell configurations with conventional square sections and achieved superior crash performance from the multi-cell structures. Zhang et al. [10–12] investigated the crashworthiness of different multi-cell sections under the axial load. Yin et al. [13] proposed that the foam-filled multi-cell structures perform better than conventional structures. Najafi and Rais-Rohani [14] studied the crash behavior of different multi-cell and multi-corner configurations under the axial quasi-static load condition. Nia and Parsapour [15] investigated the energy absorption of simple and multi-cell square tubes and found

\* Corresponding authors.

E-mail addresses: [gaoyunkai@tongji.edu.cn](mailto:gaoyunkai@tongji.edu.cn) (Y. Gao), [fangjg87@gmail.com](mailto:fangjg87@gmail.com), [jianguang.fang@uts.edu.au](mailto:jianguang.fang@uts.edu.au) (J. Fang).

that adding partitions at the corners helps to improve the crashworthiness. Qiu et al. [16] proposed four multi-cell hexagonal tubes and found that the multi-cell section with ribs connecting the internal and external walls outperforms other multi-cell structures. Qiu et al. [17] compared the Pareto frontiers of four multi-cell hexagonal tubes based on analytical solutions. Fang et al. [18] investigated the crashworthiness of four multi-cell square tubes under both axial and oblique loads. Additional studies [10,11,19–28] also proved the superiority of multi-cell tubes over single-cell counterparts under the compression load. However, most of the studies were based on predefined multi-cell cross-sectional configurations, making it difficult to systematically investigate the optimal material distribution and further to explore the most efficient cross-sections. In this study, we use the topology optimization method to fully explore the possible design candidates and excavate the maximum potential of the multi-cell energy absorber.

In real-world collisions, the energy absorbers in a vehicle may be subjected to multiple loading cases, such as frontal, side and rear collisions [29]. Therefore, the vehicle crashworthy structure is expected to have at least satisfactory performance under multiple loading cases. In general, axial compression and bending loading cases are the two most common types of loads for vehicle structures. For example, frontal rails, crash boxes, and other frontal components are required to absorb energy efficiently under compression loads, while side-door beams, door sills, B-pillars and other side structures are designed for bending loads. The above-mentioned studies mainly focused on the crashworthiness of multi-cell structures under the axial load. To consider the bending load condition, Wang et al. [30] investigated the bending resistance of multi-cell square tubes and found that the number of partition plates significantly affects the bending resistance. However, the tubes with more partition plates do not necessarily have higher energy absorption efficiency. Yin et al. [31] demonstrated that the foam-filled multi-cell thin-walled structure (FMFS) with nine cells had a better performance than other cross-sectional configurations under the lateral load. Guo and Yu [32] explored the dynamic three-point bending behavior of foam-filled double cylindrical tubes and indicated that they performed better than the traditional single tubes in terms of specific energy absorption. Fang et al. [33] introduced axial and two transverse foam grading configurations and compared their crashworthiness subjected to lateral impact loading and found that the axial foam grading tube outperformed the other two configurations.

However, the majority of the previous work for crashworthiness design focused solely on either the axial or bending load conditions, which significantly narrows the application of the designed structures [29]. To address this issue, this paper will conduct topology optimization under multiple loading cases based on a modified particle swarm optimization (PSO) algorithm. PSO, which was proposed by Kennedy and Eberhart in 1995 [34,35], is a non-gradient approach that has proved to be suitable for solving highly non-linear problems such as crashworthiness. To avoid obtaining the local optima and to improve the performance of the algorithm, a number of different PSO algorithms have been proposed. To this end, some researchers [36–38] implemented diversity control to decline the tendency of swarms to converge to local optima. Other studies investigated the adaptive PSO parameters [39–41] to respond to the environmental information, or some have proposed a hybrid technique [42,43] with other search approaches to take advantage of both strengths. However, few studies take into account the effect of the constraint in the PSO. In the crashworthiness design case, it was revealed that the optimum design tends to be located on the boundary of the mass constraint [44]. Therefore, a binary PSO algorithm is enhanced by using the mass constraint to guide the moving directions of the particles. In the paper, the topology optimization by using the binary PSO is a further study of our previous topology optimization for out-of-plane crushing of square multi-cell tubes [44].

The rest of this paper is organized as follows. First, Section 2 describes the finite element model of the multi-cell structures under the two loading cases, while Section 3 proposes a modified particle swarm optimization algorithm. Section 4 describes the employment of the modified particle optimization algorithm used to conduct topology optimization for five selected configurations. The optimum designs obtained by the algorithm are then compared for the two loading cases. Finally, the paper will be summarized with results and conclusions in Section 5.

## 2. Description of topology optimization for multi-cell hexagonal tube

### 2.1. Finite element (FE) model

According to Alavi Nia and Parsapour [45], a hexagonal section can absorb more energy than a triangular or square section with the same mass and may be a better choice for an energy absorber. The cross-sectional configurations of multi-cell hexagonal tubes considered in this study are depicted in Fig. 1. The first three configurations are proposed based on the findings of our previous studies [16,17]. Sections 4 and 5 are composed of equally sized triangular cells (see Fig. 1). The length of these tubes is 300 mm. The width of the outer wall is 36 mm. The thickness of the outer wall is 0.5 mm for all the five sections. To maintain the same mass of the initial sections, the thicknesses of the inner ribs are set to be 0.5 mm, 0.4 mm, 0.36 mm, 0.39 mm, and 0.3 mm for Sections 1–5, respectively. From a topological point of view, the first three and the last two may appear identical, varying only in cell density. However, including more cells provides a greater chance of reaching the optimal design, but at the sacrifice of computational efficiency. The tradeoff between these two factors may need to be made in a real-life engineering application.

Axial compression and lateral bending loadings were applied to the above-mentioned multi-cell hexagonal tubes by using the explicit nonlinear finite element code, LS-DYNA [46]. For the axial compression loading condition (Fig. 2a), the top end of the tube was impacted by the striker with a mass of 600 kg at an initial velocity of 15 m/s, while the bottom end was restrained to the rigid base. Fig. 2b displays the lateral bending condition, where the two ends of the tube were

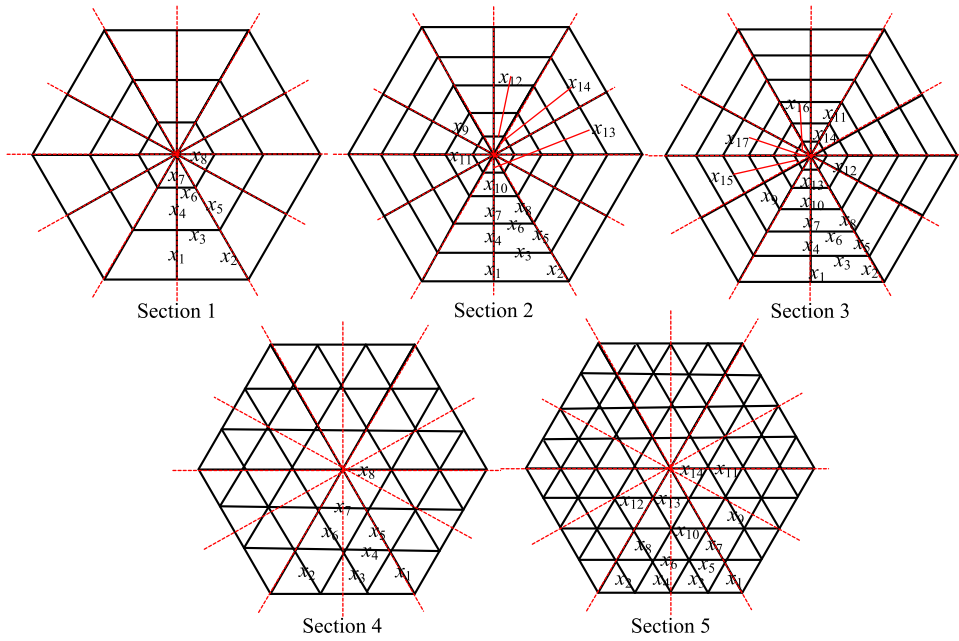


Fig. 1. Design variables of multi-cell hexagonal tubes for five different initial sections.

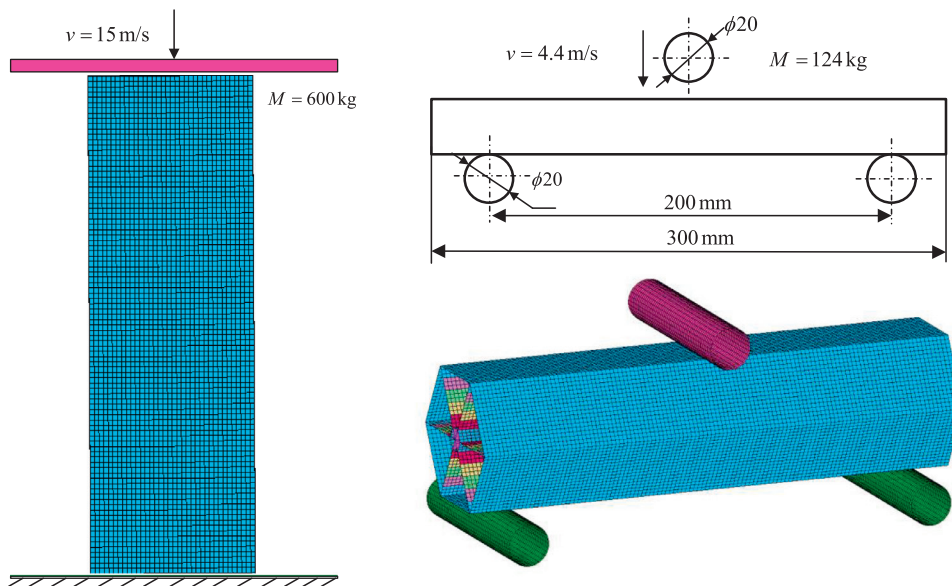


Fig. 2. Finite element model under two loading conditions: (a) axial compression and (b) lateral bending.

supported by the rigid body and the center was impacted by a rigid punch with a mass of 124 kg at an initial velocity of 4.4 m/s. The distance between two rigid supports was 200 mm. The diameters of both punch and supports were 20 mm. Belytschko-Lin-Tsay reduced integration shell elements [47] with five integration points through the thickness was adopted to model the tube's outer and inner rib walls. The hourglass control was employed to avoid spurious zero energy deformation modes. Based on a mesh convergence study, the mesh size of tube specimens for the compression bending loading case was determined as 1.5 mm (see Fig. 3a) and for the bending loading case was 2 mm (see Fig. 3b). "Automatic node to surface" option was utilized to simulate the interfaces between the tube and the striker and also between the tube and the rigid support. The other contact option "Automatic single surface" was used to model the contact between the tube's outer walls and inner ribs, thus to avoid interpenetration during buckling. The values of the Coulomb friction coefficient for all contact surfaces were set at 0.15 [12].

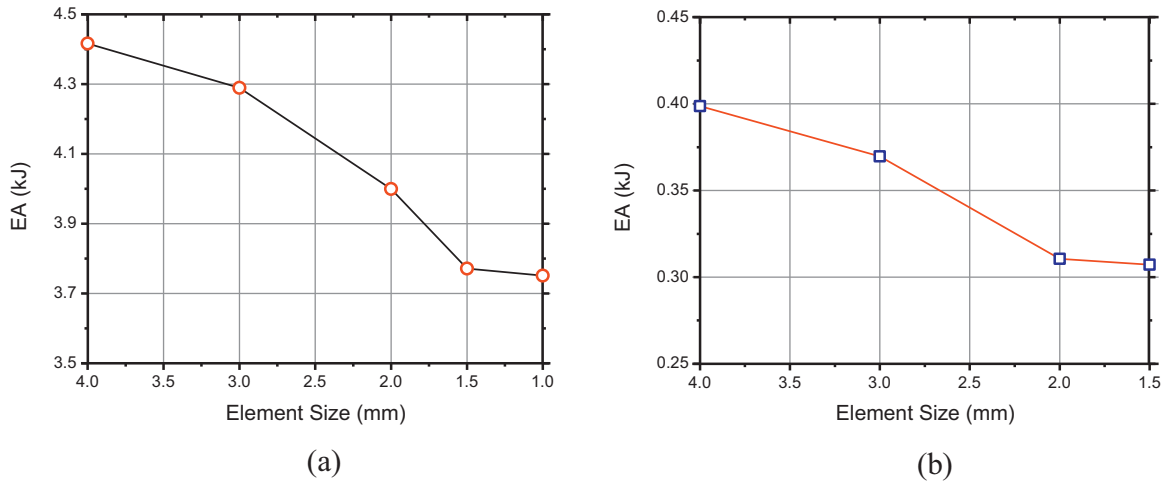


Fig. 3. Mesh convergence study for (a) axial compression loading case and (b) lateral bending loading case.

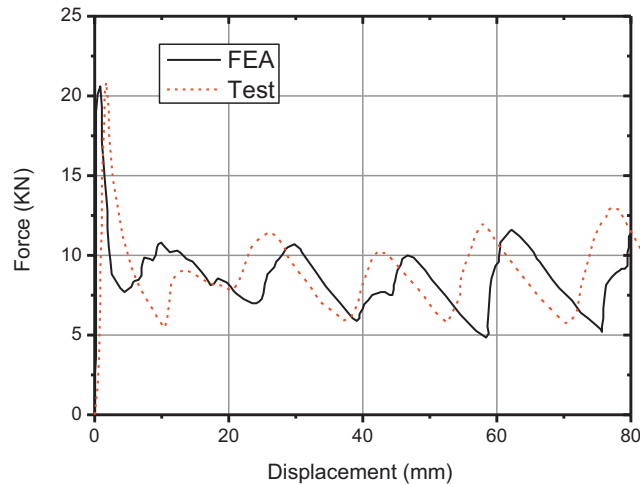


Fig. 4. Comparison of impact force versus displacement curves between FE simulation and experimental tests [12] under quasi-static axial crushing.

The tube is made of aluminum with the following mechanical properties: Young's modulus = 69 GPa, Poisson's ratio = 0.3, density = 2580 kg/m<sup>3</sup>, initial yield strength = 80 MPa and the ultimate strength = 173 MPa. The aluminum was assumed insensitive to the strain rate [33] and was modeled using an elastic-plastic material model 123 in LS-DYNA [25].

To validate the FE modeling technique, the simulation result of the single-wall hexagonal tube model under quasi-static axial compression loading was compared with its theoretical solution. The cross-sectional dimensions and length of this tube were the same as initial topology sections and its thickness was set as 1.93 mm to maintain the same mass with initial topology sections. According to Zhang and Zhang [12] and Qiu et al. [17], the analytical solutions of the average force for the single hexagonal tube can be expressed as,

$$P_m = \frac{26}{k} \sigma_0 B^{0.2} t_1^{1.8} \quad (1)$$

where the  $\sigma_0$  denotes the flow stress of the material, and  $B$  is the half length of the width.  $t_1$  is the wall thickness of the tube. Based on the above equation, the average reaction force for this single hexagonal tube was calculated as 28.55 kN when the ratio of the effective crush distance to initial length ( $k$ ) was set as 0.7. The average force obtained from the simulation model was 27.39 kN. It was observed that the relative error between the simulation model and analytical solution of average force was within 5%. In addition to the analytical solution, an experimental test reported in the literature [12] was used to validate the FE model for the single-wall hexagonal tube. The setup in the simulation was the same as that in the experimental test. As shown in Fig. 4, the force–displacement curve in the FE simulation is in good agreement with the experiment. Therefore, the FE modeling technique in this paper is considered sufficiently accurate for further topology optimization.

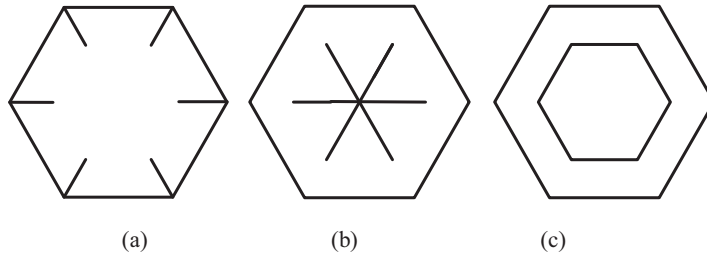


Fig. 5. Unconnected designs: (a) Type A; (b) Type B; (c) Type C.

2.2. Description of topology optimization problem

As an energy absorber, the tube is expected to absorb as much energy as possible to reduce the kinetic energy transmitted to the occupants. Therefore, energy absorption ( $EA$ ) is a commonly used crashworthiness design criterion,

$$EA(d) = \int_0^d F(s) ds \tag{2}$$

where  $d$  is the crash displacement and  $F(s)$  is the instantaneous impact force at the crash distance  $s$ . In this study,  $EA_c$  denotes the energy absorption under compression and is obtained when  $d$  is equal to 120 mm.  $EA_b$  is the energy absorption under bending when  $d$  is 40 mm. In order to normalize the energy from the two loading cases, the following dimensionless efficiency coefficients  $EA'_c$  and  $EA'_b$  are introduced:

$$EA'_c = \frac{EA_c - EA_c^L}{EA_c^U - EA_c^L} \tag{3}$$

$$EA'_b = \frac{EA_b - EA_b^L}{EA_b^U - EA_b^L} \tag{4}$$

where  $EA_c^U$  and  $EA_c^L$  are the maximum and minimum, respectively, of  $EA$  for the axial compression loading case, while  $EA_b^U$  and  $EA_b^L$  denote the maximum and minimum, respectively, of energy absorption for the lateral bending loading case. Thus,  $EA'_c$  and  $EA'_b$  will vary between 0 and 1.

To take into account the effects of different loading cases, the weight factors  $\lambda_c$  and  $\lambda_b$  are introduced to reflect the relative importance of individual  $EA'_c$  and  $EA'_b$ , and the sum of the weight factors for the two loading cases is equal to 1:

$$\lambda_c + \lambda_b = 1 \tag{5}$$

The weight factors can be determined based on the usage of tube and/or experience. In this paper, different combinations of weight factors will be discussed in Section 4.

The objective of topology optimization herein is to enhance the normalized energy absorption  $EA'_c$  and  $EA'_b$  while maintaining the total mass ( $m$ ) under a threshold to achieve excellent crashworthiness and meet a lightweight criterion. Therefore, the optimization problem of multi-cell hexagonal tubes can be expressed as:

$$\begin{cases} \min -\lambda_c EA'_c(x_1, x_2, \dots, x_n) - \lambda_b EA'_b(x_1, x_2, \dots, x_n) \\ \text{s.t. } m(x_1, x_2, \dots, x_n) \leq m_0 w \\ f_{connectivity}(x_1, x_2, \dots, x_n) \neq 0 \\ x_1, x_2, \dots, x_n \in \{0, 1\} \end{cases} \tag{6}$$

where  $x_i$  ( $i = 1, 2, \dots, n$ ) contains the binary design variables.  $x_i = 1$  means that the  $i$ th member is present and  $x_i = 0$  when the member is absent.  $m$  is the mass of the current design, while  $m_0$  is the maximum mass when all  $x_i = 1$ . The thickness of the outer wall was not a design variable and was fixed as 0.5 mm in this study. The mass ratio  $w$  was used to constrain the mass of the design, which was defined as the ratio of the mass of the optimum design to the maximum mass  $m_0$  of the fully-populated design. To satisfy the lightweight requirement, the mass of the multi-cell structures was constrained in the topology optimization process. In this study, three mass ratios were considered:  $w = 30\%$ ,  $40\%$  and  $50\%$ .

In addition to the mass constraint, the connectivity condition was also taken into account in the design. Generally speaking, there are three kinds of disconnected cases as illustrated in Fig. 5.  $f_{connectivity}$  denotes the connectivity conditions for the multi-cell structure and was checked before the FE analysis. A penalty factor was applied to the design that violates the mass constraint or connectivity requirement. Overall, the fitness value for different designs in the optimization process can be evaluated as

$$fit_i = \begin{cases} 50(m_i - m_0 w), m_i > m_0 w \\ -\lambda_c EA'_c - \lambda_b EA'_b, m_i \leq m_0 w \cap f_{connectivity}(x_1, x_2, \dots, x_n) \neq 0 \\ 1000, m_i \leq m_0 w \cap f_{connectivity}(x_1, x_2, \dots, x_n) = 0 \end{cases} \tag{7}$$

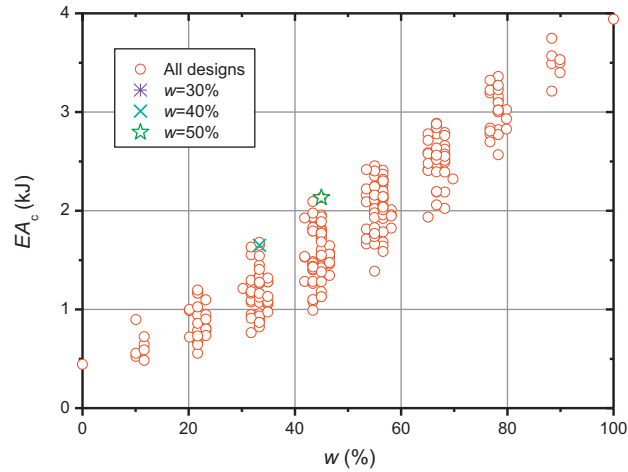


Fig. 6. Energy absorption versus mass ratio under axial compression load for Section 1.

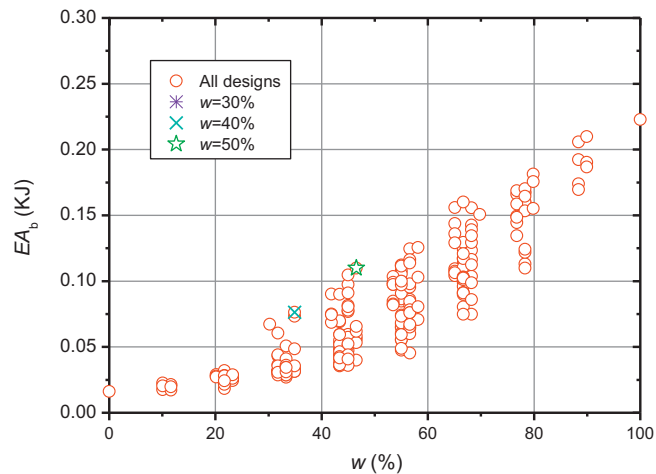


Fig. 7. Energy absorption versus mass ratio under lateral bending load for Section 1.

### 3. Modified particle swarm (PSO) algorithm for topology optimization of multi-cell tubes

To investigate the relationship between optimum designs and their mass constraints, Section 1 with 8 design variables (see Fig. 1) was studied as an example. We performed the numerical analysis for all 256 ( $= 2^8$ ) possible designs under both axial compression and lateral bending loads. The energy absorptions of these designs under the two loading cases are depicted in Figs. 6 and 7. Generally speaking, a large mass ratio  $w$  can absorb more energy. Specifically, the optimal solutions with the mass constraint  $w=30\%$ ,  $40\%$ , and  $50\%$  are all close to the mass constraints, but not exactly on the constraint boundary as marked in Figs. 6 and 7. This is due to the discrete property of this binary topology optimization problem. For this reason, the optimums tend to be located on the boundary of the mass constraint in the feasible design space. It was observed that there is no connected solution for Section 1 with the mass constraint of  $w=30\%$  because the allowed mass ratio is too low. To accelerate the optimization process, the mass effect was considered in the velocity update function of PSO. By pushing the optimal solution to the mass constraint boundary, it provides a higher chance of finding the optimum solution.

In this study, a modified binary particle swarm optimization (PSO) was used to find the optimal solutions for different multi-cell tubes. This algorithm works by producing a population of candidate solutions (namely particles), which have been successfully employed to solve real-world problems [48–53]. Generally, these particles move around with the guidance of their local and global best positions within the search space to find the optimums. The velocity of particles' motion for the original PSO can be written as

$$v_{i,d+1} = \omega \cdot v_{i,d} + \varphi_p r_p (p_{i,d} - x_{i,d}) + \varphi_g r_g (g_{i,d} - x_{i,d}) \quad (8)$$

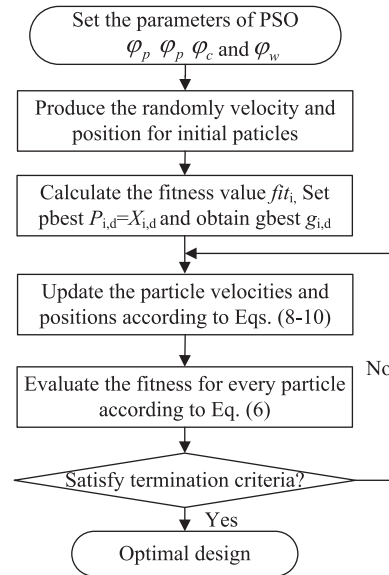


Fig. 8. Flowcharts of modified PSO algorithm.

where  $v_{i,d+1}$  is the updated velocity for the  $i$ th particle at the  $(d+1)$ th iteration, and  $x_{i,d}$  is the current position of the particle. The previous best design,  $p_{i,d}$ , and the global best design,  $g_{i,d}$ , are defined as the local and global optimums, respectively.  $r_g$  and  $r_p$  are random numbers between 0 and 1, which is used to introduce the stochastic process.

Based on the observations in Figs. 6 and 7, the mass constraint effect is taken into account to improve the convergence of the algorithm. Therefore, for the modified PSO algorithm, the particle velocity can be calculated by

$$v_{i,d+1} = \varphi_w \cdot v_i + \varphi_p r_p (p_{i,d} - x_{i,d}) + \varphi_g r_g (g_{i,d} - x_{i,d}) + \varphi_c (m_0 w - m) / m_0 w \tag{9}$$

where the last term moves the particle toward the mass constraint boundary. In this study, the parameters for the PSO algorithm were set as  $\phi_p = \phi_g = 1.25$ ,  $\phi_c = 1.00$ , and the inertial weight  $\phi_w = 0.73$ . The particle positions for binary variables can be determined by [54,55]

$$x_{i,d+1} = \begin{cases} 1 & \text{if } r_i < \text{sig}(v_{i,d+1}) \\ 0 & \text{otherwise} \end{cases} \tag{10}$$

where  $r_i$  is a random number between 0 and 1, and  $\text{sig}(v_{i,d+1})$  can be calculated as

$$\text{sig}(v_{i,d+1}) = \frac{1}{1 + e^{-v_{i,d+1}}} \tag{11}$$

As depicted in Fig. 8, the procedure of modified PSO algorithm is described as:

- (1) Set the PSO parameters, e.g. population size, acceleration factors, maximum generation, etc.;
- (2) Produce random values for initial velocity  $v_{i,d}$  and position  $x_{i,d}$ . Then, calculate the fitness value  $fit_i$ ; initialize the iteration number  $t=0$ , set  $p_{i,d} = x_{i,d}$ , and obtain the optimum position  $g_{i,d}$ .
- (3) Update the particle velocities  $v_{i,d+1}$  utilizing Eq. (9).
- (4) Update the particle positions  $x_{i,d+1}$  according to Eqs. (10) and (11) and calculate their fitness function values  $fit(x_{i,d+1})$ . If  $fit(x_{i,d+1}) \leq fit(g_{i,d})$ , then  $p_{i,d} = x_{i,d}$ ; otherwise  $g_{i,d} = x_{i,d}$ .
- (5) Check if the termination criteria are met: if so, terminate the optimization process; otherwise  $t = t + 1$  and return to Step (3).

To check the performance of the proposed modified PSO algorithm, the optimization results obtained from the original and modified PSO were compared in Table 1. The success rate represents how many runs can obtain the global optimum out of five repeated runs, which was used to evaluate the performance of the original and modified PSO algorithms. It was observed from Table 1 that at least one run (out of five) can obtain the global optimum for both algorithms. More importantly, the modified PSO was found more robust in terms of the worst and average objective values and has a high success rate. In this study, the optimization was performed by directly coupling the FE model, which calls the FE analyses for function evaluations. Thus, the modified PSO is able to help to reduce the computational cost considerably by reducing the number of FE analyses.

The flowchart of the optimization process is depicted in Fig. 9. The highlighted box in the figure is the modification of the original PSO. This optimization algorithm is mainly implemented in Matlab, coupled with finite element analysis using

**Table 1**  
Comparison of the original and modified PSO for Section 2 under compression loading case.

	w = 30%		w = 40%		w = 50%	
	Modified PSO	Original PSO	Modified PSO	Original PSO	Modified PSO	Original PSO
Best (kJ)	1.35	1.35	1.85	1.85	2.30	2.30
Average (kJ)	1.18	1.85	1.67	1.67	2.22	2.13
Worst (kJ)	0.93	1.34	1.38	1.38	2.02	2.01
Success rate	3/5	1/5	3/5	3/5	3/5	1/5

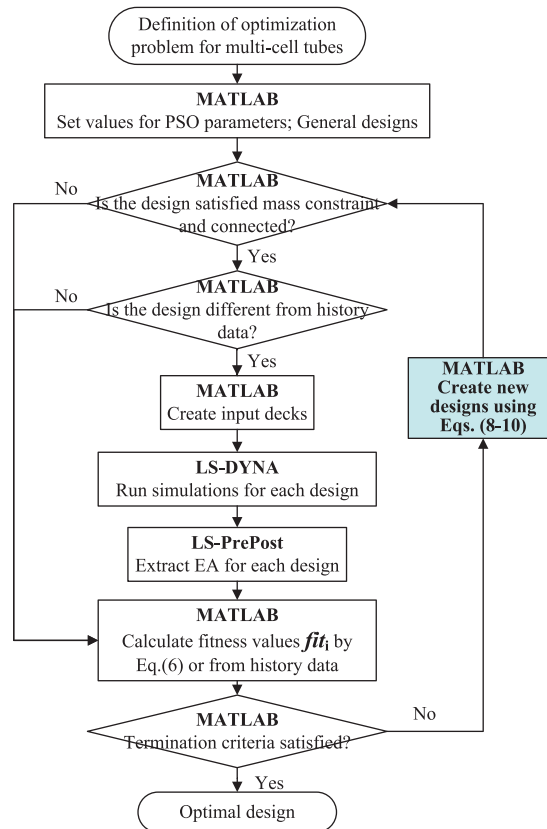


**Fig. 9.** Flowcharts of topology optimization for multi-cell tubes.

LS-DYNA. Since the binary design variables can only have a finite number of possible combinations, the history data for the previous designs are stored and checked every time before running an FE model, which can significantly reduce the computational time in the later cycle of the optimization process.

#### 4. Topology optimization of multi-cell sections under axial and lateral loading cases

In this paper, the weighting factors in Eq. (6) were changed to consider the different loading conditions: the axial compression loading case (Case I), the lateral bending loading case (Case II) and the multiple loading case (Case III).

Case I:  $\lambda_1 = 1.0$ ,  $\lambda_2 = 0.0$

Case II:  $\lambda_1 = 0.0$ ,  $\lambda_2 = 1.0$

Case III:  $\lambda_1 = 0.5$ ,  $\lambda_2 = 0.5$

##### 4.1. Case I: optimization results under axial compression loading case

The energy absorption values  $EA$  and the optimal solutions for the single wall and multi-cell structures for Sections 1–3 are depicted in Fig. 10. The optimization was conducted based on the dimensionless efficiency coefficients  $EA'$ , but for the discussion purpose, energy absorption  $EA$  was used in Section 4. The energy absorption values  $EA$  were obtained

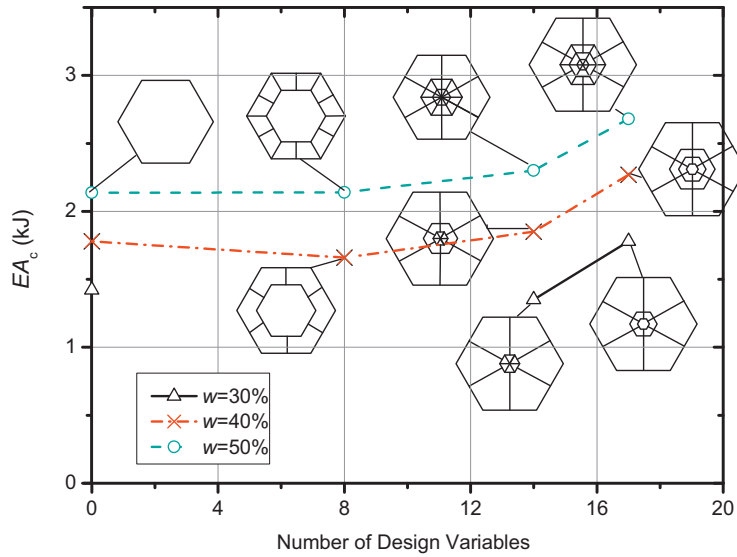


Fig. 10. Optimization results for Sections 1–3 under compression load.

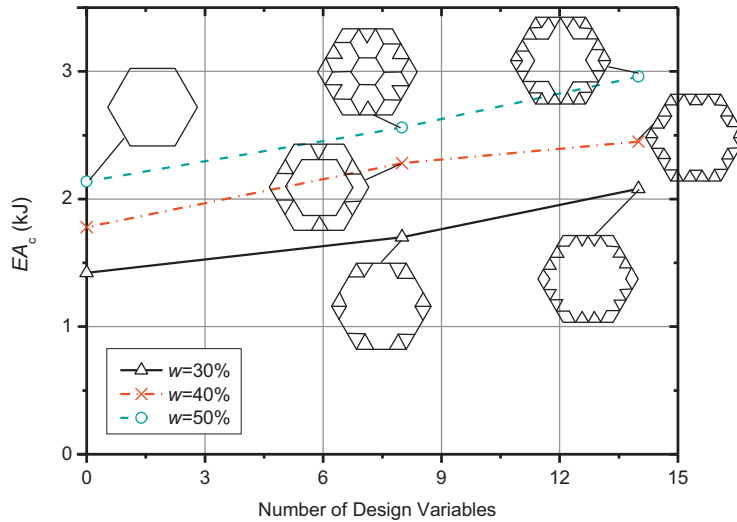


Fig. 11. Optimization results for Sections 4–5 under compression load.

from the dimensionless parameters  $EA'$  based on Eqs. (3) and (4). As shown in Fig. 10, the number of design variables denotes the different structures: single wall structure (0 design variable), Section 1 (8 design variables), Section 2 (14 design variables) and Section 3 (17 design variables). Generally speaking, energy absorbing capacity increases with the increase of the number of design variables. However,  $E_c$  of Section 1 is smaller than that of the single wall structure due to the discrete distribution of mass for multi-cell structures. Section 1 cannot fully take advantage of the mass within the allowable limit, as the single wall structure is exactly at the mass constraint. Specifically, as shown in Fig. 6, with the mass constraint  $w=40\%$ , the mass ratio for the optimal solution is only 33.3%. Obviously, the greater mass constraint provides more design candidates and can achieve better crashworthiness performance (see Fig. 10). From Fig. 10, the optimums tend to distribute their material outwards and also create more intersections between the inside rib walls.

The optimal solutions of Sections 4 and 5 and their energy absorptions are plotted in Fig. 11. Section 4 has 8 design variables and Section 5 has 14 design variables. It was observed that the optimal solution of Section 4 (8 design variables) is better than Section 2 (14 design variables), because the basic element of Section 4 is an equal-sized triangular cell, while the basic element of Section 2 is not. For Section 2, as shown in Fig. 1, some ribs are much longer than others, which makes it hard to fully use the allowed mass and difficult to connect the outside wall in order to satisfy the connectivity requirement. Generally speaking, Section 3 helps to make the full use of the allowed mass and distributes the material outward as much as possible. As shown in Fig. 11, the final optimums arrange their materials at the corners and the middle of the outer wall. This is because the rib walls located at the corners can produce a higher force and thus absorb more energy. The

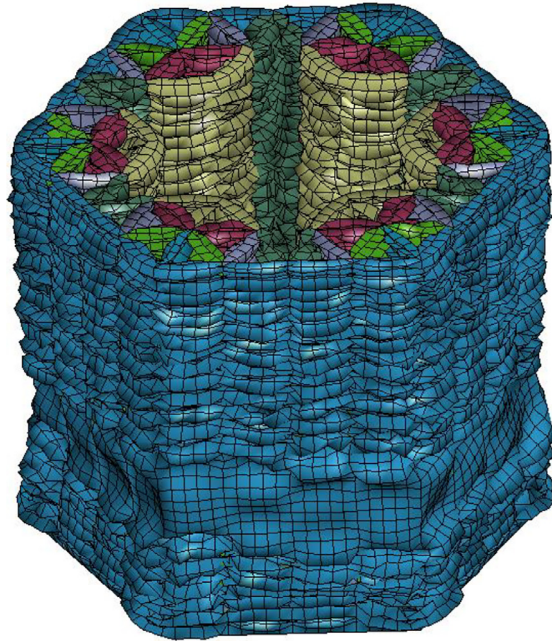


Fig. 12. Deformation mode of optimum with mass constraint 50% for Sections 5 under compression load.

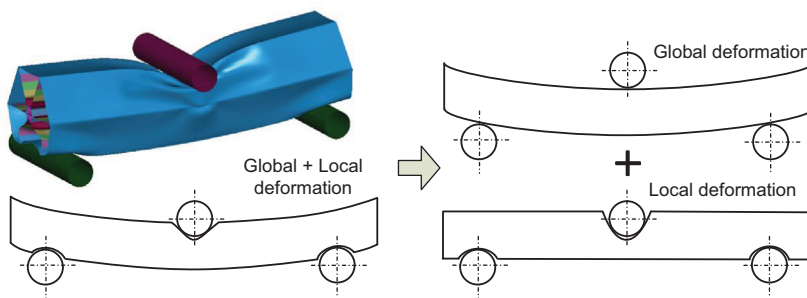


Fig. 13. Deformation mode under the lateral bending load condition.

other way to enhance energy absorption is to produce more intersections. From Fig. 10, Sections 2 and 3 have a number of intersectional ribs inside of the tube. Through the comparative study of five multi-cell structures, Section 5 performs the best in crashworthiness because it can make full use of the allowed mass and thus has more feasible design candidates. Fig. 12 shows the deformation mode of the optimum for Section 5 under the compression load, which is the best configuration under the mass constraint of  $w = 50\%$ . It was observed that this optimum solution yields a stable progressive collapse mode, which is considered as an efficient mode for energy absorption. It was also noticed the wavelength for this configuration is relatively small and thus more folds were produced in the axial crushing process, which also results in more energy absorption.

#### 4.2. Case II: optimization results under lateral bending loading case

For the lateral bending loading case, the energy absorbing capacity is not only associated with the local deformation of the contact area, but also with the global deformation of bending as depicted in Fig. 13. While the local deformation is more dependent on the local stiffness of the tube, the global deformation is more affected by the moment of inertia. To clarify the relationship between energy absorption and the moment of inertia under the lateral loading case, they are plotted in Fig. 14 for Sections 1–3 and Fig. 15 for Sections 4–5. In these figures, the dashed lines show the moment of inertia, whose values are shown in the right ordinate, while the solid lines show energy absorption (EA), whose values are shown in the left ordinate. It was observed that the single wall tubes have a greater moment of inertia than the multi-cell tubes for the following two reasons. The first reason is that the mass of the single wall structure is the same as the mass constraint, but the mass of the multi-cell tube is discrete and may be far less than the mass constraint. The other reason is that the mass of the single wall tube is all distributed at the outer wall, which increases the moment of inertia. However, the single wall

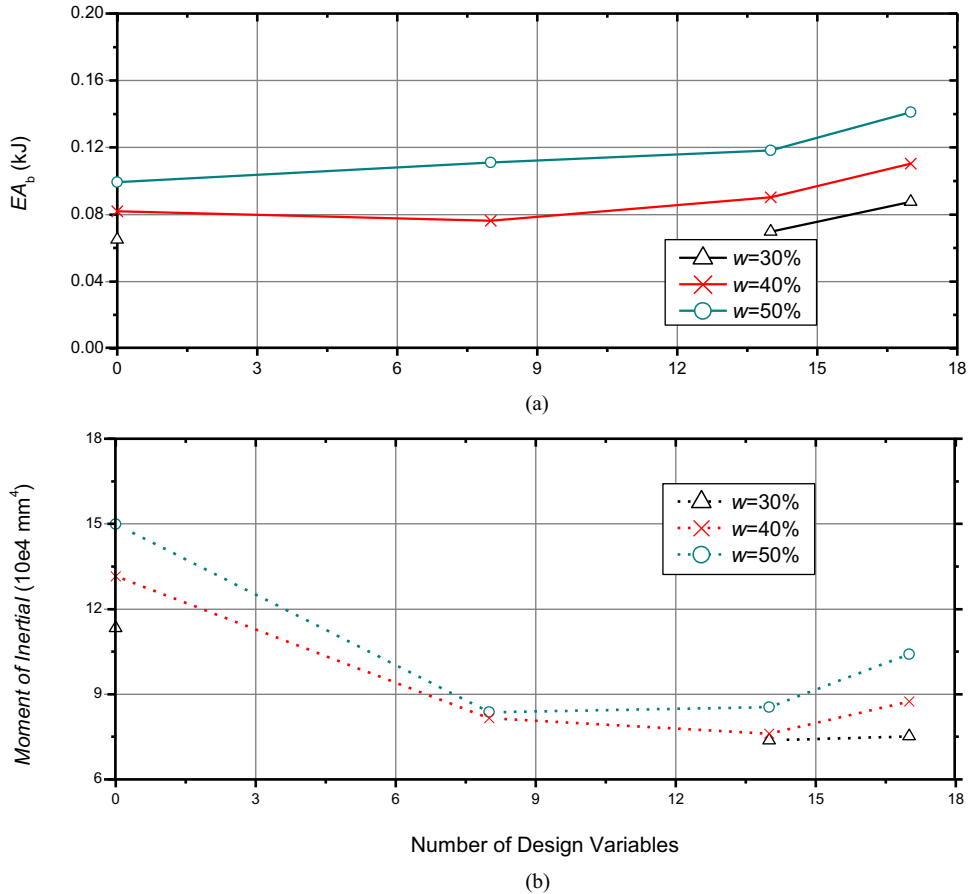


Fig. 14. Comparison of energy absorption and moment of inertia for single wall tube and tubes with Sections 1–3 (a) energy absorption (b) moment of inertia.

tube performs worse in resisting the local deformation, which is another important factor in the lateral impact case. For the multi-cell structures, all the optimum designs have diagonal components which help to resist local deformation. In these cases, the energy absorption abilities are more affected by the moment of inertia (from Figs. 14 and 15).

Furthermore, the energy absorptions of the optimal results are plotted in Fig. 16 for Sections 1–3 and Fig. 17 for Sections 4–5. It was observed that diagonal components are always present in all of the optimal designs. These diagonal elements can increase the resistance to local deformation and thus enhance the energy absorption under lateral bending. Similar to the optimums under the axial compression load, the optimums under lateral bending tend to have a large mass. Again, a greater mass constraint provides more feasible designs.

From the above-mentioned discussion, the optimization tries to move the material outward under both the axial compression and lateral bending cases, while only the bending load tries to have more diagonal members in the section to resist local deformation of the contacting area. It should be noted that the optimal solutions show more improvement under the bending loading case than under the axial loading condition. This is because, under the compression load, more mass distributed on the outside of the tube will result in better performance. As a result, even the single wall structure performs well. However, in the case of bending, the diagonal elements can give considerable support for the whole section to resist the local deformation. In this case, the multi-cell is a significant improvement over the single wall structure.

#### 4.3. Case III: optimization results under multiple loading cases

In the previous sections, the multi-cell tubes are optimized based on individual axial compression and lateral bending loading cases. However, in practice, it would be more beneficial to determine the optimal sections for multiple loading cases, which is the aim of this Section. For simplicity, the weight factors are determined to be 0.5 for each loading case. The realistic determination of weight factors for different load cases should follow the statistical data and/or occurrence frequency of the application component in real life [18], which is however beyond the scope of this study.

Table 2 compares the optimal sections under individual and multiple loading cases. It was observed that with the mass constraint of  $w=30\%$ , the optimal designs under multiple loading cases are the same as the optimal designs for the com-

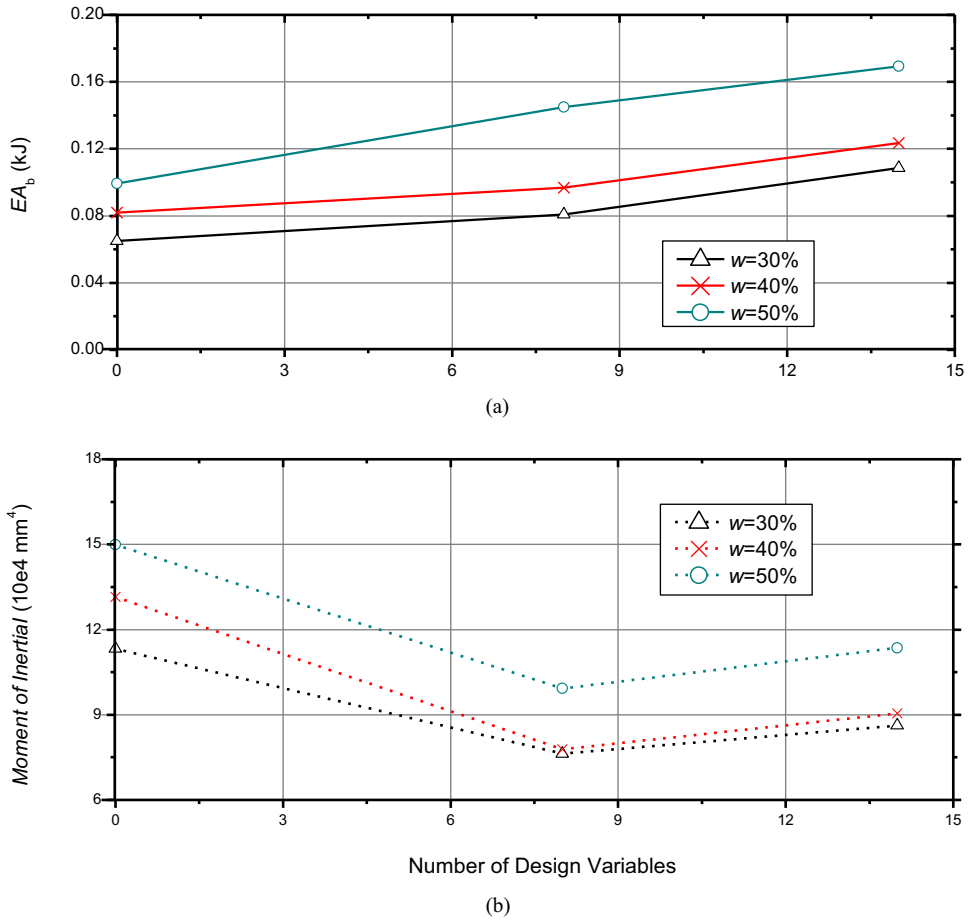


Fig. 15. Comparison of energy absorption and moment of inertia for single wall tube and tubes with Sections 4–5 (a) energy absorption (b) moment of inertia.

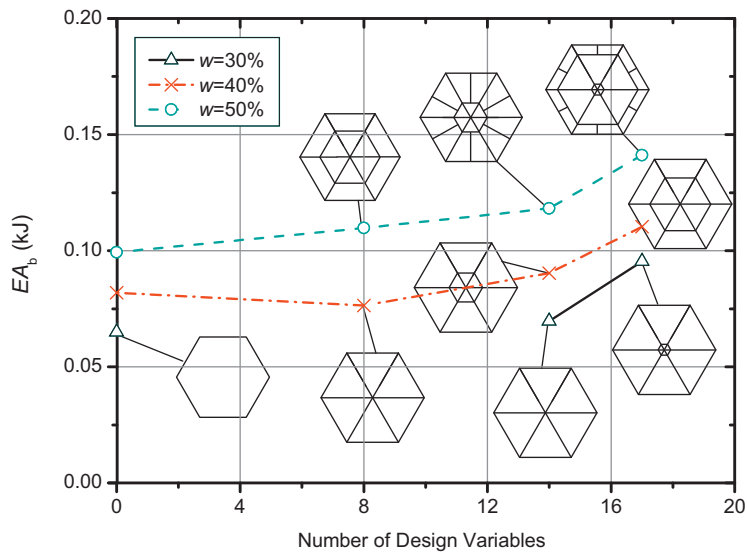
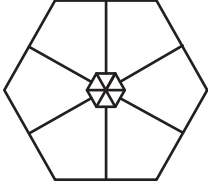
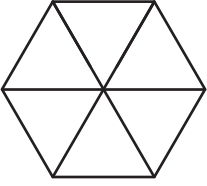
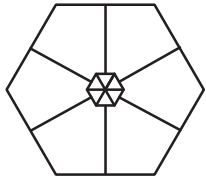
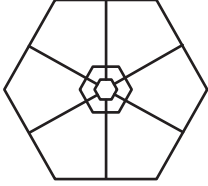
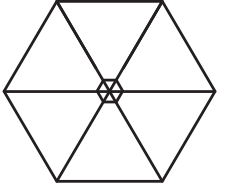
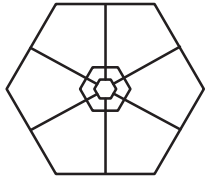
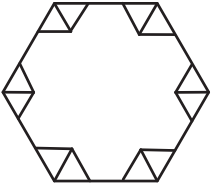
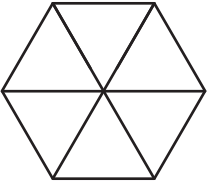
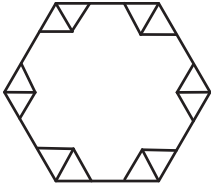
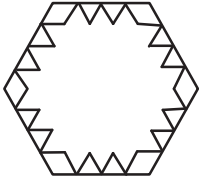
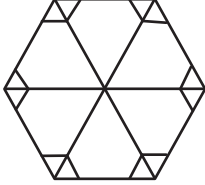
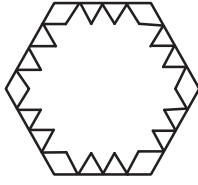
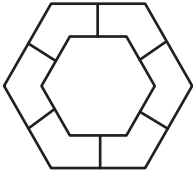
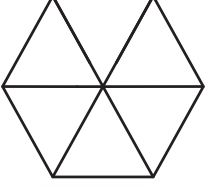
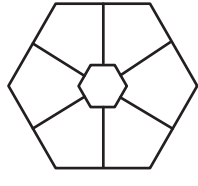
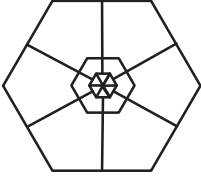
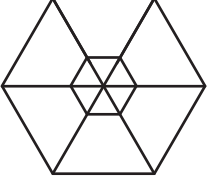
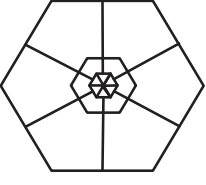
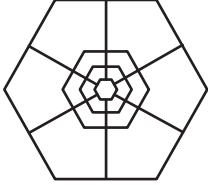
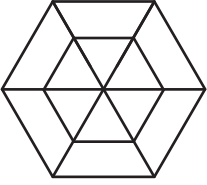
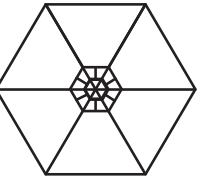


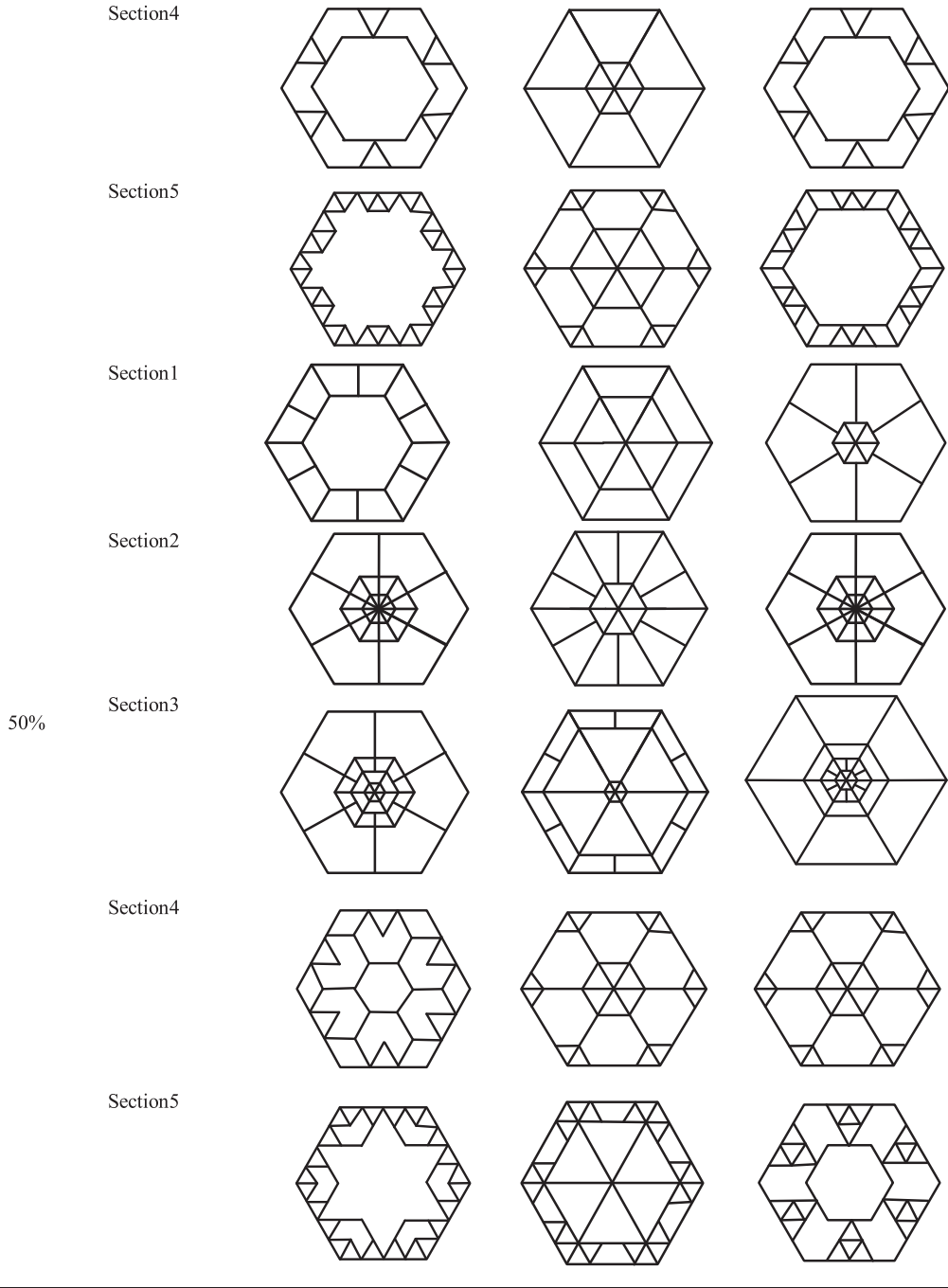
Fig. 16. Optimization results and optimal designs for Sections 1–3 under bending.

**Table 2**  
Final optimal designs under three different loading cases.

Mass ratio $w$	Section name	Optimums under compression load	Optimums under bending load	Optimums under multiple load
30%	Section1		No connected solution	
	Section2			
	Section3			
	Section4			
	Section5			
40%	Section1			
	Section2			
	Section3			

(continued on next page)

Table 2 (continued)



pression loading case. This is because that placing of material outward can strengthen the interaction between the outside wall and inside wall as well as improve the resistance of global bending by increasing the moment of inertia. Therefore, the optimum solution of the compression loading case performs reasonably well for the bending load. But the diagonal elements in the optimal designs of the bending loading case cannot contribute much in the compression loading case. For  $w = 40\%$  and  $50\%$ , the optimums are either the same as the design under compression load or a combination of the optimal designs of the compression load and bending load. It indicates that with a low mass ratio, the compression load is dominant, while with a high mass ratio, both loading cases affect the optimal design.

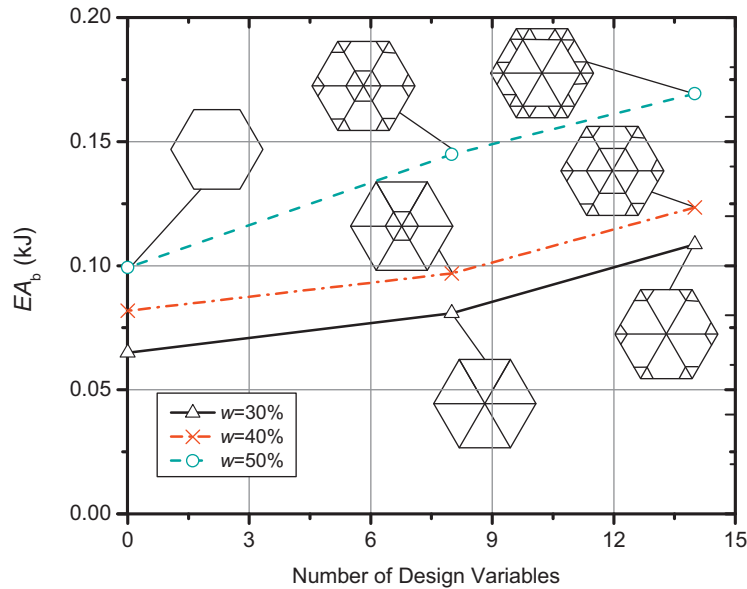


Fig. 17. Optimization results and optimal designs for Sections 4–5 under bending.

In the past, the difficulty in manufacturing complex components obtained from topology optimization prevented their usage in industrial application. However, the development of new manufacturing skills can fill this gap [56]. First, the state-of-the-art extrusion process could manufacture arbitrary cross-sectional members relatively easily without a significant increase in cost. This would make fabrication of multi-cell tubes with complex cross-sectional configurations straightforward [9]. In addition, Additive Manufacturing (AM) is capable of translating the complex solid model data into a 3D physical model [57]. Thus, more complex cross-sectional configurations can be manufactured by utilizing this technology.

## 5. Conclusions

In this study, the cross-sectional configurations of five multi-cell hexagonal tubes were topologically optimized by utilizing a modified particle swarm optimization (PSO) under multiple loading cases. The finite element model, which was constructed based on the non-linear finite element code LS-DYNA, was directly coupled with the modified PSO algorithm, aiming to maximize the energy absorption ( $EA$ ) subject to the connectivity and mass constraints. By taking Section 2 under compression loading case as an example, the modified PSO was found to be robust in terms of the worst and average objective values and success rate of obtaining the global optimum. This algorithm was then utilized in the crashworthiness design of multi-cell tubes under axial compression and lateral bending cases, where the presence of the inner ribs was considered as design variables.

By comparing the optimal solutions, multi-cell tubes were found to perform better than the single wall tubes under both compression and bending loading cases. For different multi-cell structures, Sections 4 and 5 (with equally sized triangular cells) performed better than Sections 1 and 2 (with multiple radial layers) with the same number of design variables and the same mass constraint. Even Section 5 (14 design variables) performs better than Section 3 (17 design variables) in some cases. Although Sections 1–3 have more intersections, which were demonstrated preferable for improving the energy absorbing capacity, the ribs located outside were much longer than the ribs located inside. Therefore, in some cases, it would be difficult to select these longer ribs while meeting the connectivity and mass constraints. Sections 4 and 5 have equally-sized cell elements and have more opportunities to distribute the material outward.

For different loading cases, optimization offered different topological configurations. Under the axial compression loadings, the optimums place the material outward to strengthen the interactions between the outside walls and inside wall and had more partitions between the rib walls. While for the bending load, the optimums had diagonal components to prevent local deformation, as well as to distribute the material outward to increase the moment of inertia and resist global bending. It is interesting to find that the optimal designs under multiple loading cases were the same as that under compression load when the mass ratio was low ( $w=30\%$ ). However, when the mass ratio became high, the optimal designs under multiple loading cases were more likely to create new configurations that combined the cross-sections of the compression load and bending load. The optimum solutions obtained from only one loading case may have inferior performances when subjected to the other loading case. By contrast, the optimum solutions of considering multiple loading cases can perform relatively well for both loading cases.

## Acknowledgment

This work was supported by The National Natural Science Foundation of China (51575399) and The National Science & Technology Program during the Thirteenth Five-Year Plan Period (2016YFB0101600). The first author is a recipient of the doctoral scholarships from China Scholarship Council (CSC). The Chancellor's Postdoctoral Research Fellowship from the University of Technology Sydney is acknowledged by the third author.

## References

- [1] Y. Xiang, Q. Wang, Z. Fan, H. Fang, Optimal crashworthiness design of a spot-welded thin-walled hat section, *Finite Elem. Anal. Des.* 42 (2006) 846–855.
- [2] Y. Liu, Optimum design of straight thin-walled box section beams for crashworthiness analysis, *Finite Elem. Anal. Des.* 44 (2008) 139–147.
- [3] J. Fang, G. Sun, N. Qiu, N.H. Kim, Q. Li, On design optimization for structural crashworthiness and its state of the art, *Struct. Multidiscip. Optim.* 55 (2017) 1091–1119.
- [4] H. Yin, G. Wen, S. Hou, K. Chen, Crushing analysis and multiobjective crashworthiness optimization of honeycomb-filled single and bitubular polygonal tubes, *Mater. Des.* 32 (2011) 4449–4460.
- [5] H. Yin, G. Wen, H. Fang, Q. Qing, X. Kong, J. Xiao, Z. Liu, Multiobjective crashworthiness optimization design of functionally graded foam-filled tapered tube based on dynamic ensemble metamodel, *Mater. Des.* 55 (2014) 747–757.
- [6] A. Alavi Nia, M.Z. Sadeghi, The effects of foam filling on compressive response of hexagonal cell aluminum honeycombs under axial loading-experimental study, *Mater. Des.* 31 (2010) 1216–1230.
- [7] L. Aktay, B.H. Kröplin, A.K. Toksoy, M. Güden, Finite element and coupled finite element/smooth particle hydrodynamics modeling of the quasi-static crushing of empty and foam-filled single, bitubular and constraint hexagonal- and square-packed aluminum tubes, *Mater. Des.* 29 (2008) 952–962.
- [8] G. Sun, T. Pang, J. Fang, G. Li, Q. Li, Parameterization of criss-cross configurations for multiobjective crashworthiness optimization, *Int. J. Mech. Sci.* 124–125 (2017) 145–157.
- [9] H.-S. Kim, New extruded multi-cell aluminum profile for maximum crash energy absorption and weight efficiency, *Thin-Walled Struct.* 40 (2002) 311–327.
- [10] X. Zhang, H. Zhang, Axial crushing of circular multi-cell columns, *Int. J. Impact Eng.* 65 (2014) 110–125.
- [11] X. Zhang, G. Cheng, A comparative study of energy absorption characteristics of foam-filled and multi-cell square columns, *Int. J. Impact Eng.* 34 (2007) 1739–1752.
- [12] X. Zhang, H. Zhang, Energy absorption of multi-cell stub columns under axial compression, *Thin-Walled Struct.* 68 (2013) 156–163.
- [13] H. Yin, G. Wen, X. Wu, Q. Qing, S. Hou, Crashworthiness design of functionally graded foam-filled multi-cell thin-walled structures, *Thin-Walled Struct.* 85 (2014) 142–155.
- [14] A. Najafi, M. Rais-Rohani, Mechanics of axial plastic collapse in multi-cell, multi-corner crush tubes, *Thin-Walled Struct.* 49 (2011) 1–12.
- [15] A. Alavi Nia, M. Parsapour, An investigation on the energy absorption characteristics of multi-cell square tubes, *Thin-Walled Struct.* 68 (2013) 26–34.
- [16] N. Qiu, Y. Gao, J. Fang, Z. Feng, G. Sun, Q. Li, Crashworthiness analysis and design of multi-cell hexagonal columns under multiple loading cases, *Finite Elem. Anal. Des.* 104 (2015) 89–101.
- [17] N. Qiu, Y. Gao, J. Fang, Z. Feng, G. Sun, Q. Li, Theoretical prediction and optimization of multi-cell hexagonal tubes under axial crashing, *Thin-Walled Struct.* 102 (2016) 111–121.
- [18] J. Fang, Y. Gao, G. Sun, N. Qiu, Q. Li, On design of multi-cell tubes under axial and oblique impact loads, *Thin-Walled Struct.* 95 (2015) 115–126.
- [19] Z. Tang, S. Liu, Z. Zhang, Analysis of energy absorption characteristics of cylindrical multi-cell columns, *Thin-Walled Struct.* 62 (2013) 75–84.
- [20] X. Zhang, G. Cheng, H. Zhang, Theoretical prediction and numerical simulation of multi-cell square thin-walled structures, *Thin-Walled Struct.* 44 (2006) 1185–1191.
- [21] W. Chen, T. Wierzbicki, Relative merits of single-cell, multi-cell and foam-filled thin-walled structures in energy absorption, *Thin-Walled Struct.* 39 (2001) 287–306.
- [22] T. Tran, S. Hou, X. Han, N. Nguyen, M. Chau, Theoretical prediction and crashworthiness optimization of multi-cell square tubes under oblique impact loading, *Int. J. Mech. Sci.* 89 (2014) 177–193.
- [23] S. Hou, Q. Li, S. Long, X. Yang, W. Li, Multiobjective optimization of multi-cell sections for the crashworthiness design, *Int. J. Impact Eng.* 35 (2008) 1355–1367.
- [24] W. Hong, H. Fan, Z. Xia, F. Jin, Q. Zhou, D. Fang, Axial crushing behaviors of multi-cell tubes with triangular lattices, *Int. J. Impact Eng.* 63 (2014) 106–117.
- [25] J. Fang, Y. Gao, G. Sun, G. Zheng, Q. Li, Dynamic crashing behavior of new extrudable multi-cell tubes with a functionally graded thickness, *Int. J. Mech. Sci.* 103 (2015) 63–73.
- [26] S. Hou, Q. Li, S. Long, X. Yang, W. Li, Design optimization of regular hexagonal thin-walled columns with crashworthiness criteria, *Finite Elem. Anal. Des.* 43 (2007) 555–565.
- [27] C.E. Augarde, A.J. Deeks, The use of Timoshenko's exact solution for a cantilever beam in adaptive analysis, *Finite Elem. Anal. Des.* 44 (2008) 595–601.
- [28] J. Paz, J. Díaz, L. Romera, M. Costas, Crushing analysis and multi-objective crashworthiness optimization of GFRP honeycomb-filled energy absorption devices, *Finite Elem. Anal. Des.* 91 (2014) 30–39.
- [29] X. An, Y. Gao, J. Fang, G. Sun, Q. Li, Crashworthiness design for foam-filled thin-walled structures with functionally lateral graded thickness sheets, *Thin-Walled Struct.* 91 (2015) 63–71.
- [30] Z. Wang, Z. Li, X. Zhang, Bending resistance of thin-walled multi-cell square tubes, *Thin-Walled Struct.* 107 (2016) 287–299.
- [31] H. Yin, Y. Xiao, G. Wen, Q. Qing, Y. Deng, Multiobjective optimization for foam-filled multi-cell thin-walled structures under lateral impact, *Thin-Walled Struct.* 94 (2015) 1–12.
- [32] L. Guo, J. Yu, Dynamic bending response of double cylindrical tubes filled with aluminum foam, *Int. J. Impact Eng.* 38 (2011) 85–94.
- [33] J. Fang, Y. Gao, G. Sun, Y. Zhang, Q. Li, Parametric analysis and multiobjective optimization for functionally graded foam-filled thin-wall tube under lateral impact, *Comput. Mater. Sci.* 90 (2014) 265–275.
- [34] J. Kennedy, R. Eberhart, Particle swarm optimization, Paper presented at IEEE International Conference on Neural Networks, Perth, Australia, IEEE Service Center, 1995.
- [35] R. Eberhart, J. Kennedy, A new optimizer using particle swarm theory, in: *Proceedings of the Sixth International Symposium on Micro Machine and Human Science*: Oct 1995, 1995.
- [36] M. Løvbjerg, T.K. Rasmussen, T. Krink, Hybrid particle swarm optimizer with breeding and subpopulations, in: *Proceedings of the Third Annual Conference on Genetic and Evolutionary Computation*, Morgan Kaufmann Publishers Inc., 2001, pp. 469–476.
- [37] T.M. Blackwell, P. Bentley, Don't push me! Collision-avoiding swarms, in: *Proceedings of the 2002 Congress on Evolutionary Computation*, 2002. CEC'02, IEEE, 2002, pp. 1691–1696.
- [38] X.-F. Xie, W.-J. Zhang, Z.-L. Yang, Dissipative particle swarm optimization, in: *Proceedings of the 2002 Congress on Evolutionary Computation*, 2002. CEC'02, IEEE, 2002, pp. 1456–1461.
- [39] Z.H. Zhan, J. Zhang, Y. Li, H.S.H. Chung, Adaptive particle swarm optimization, *IEEE Trans. Syst. Man, Cybern. Part B (Cybern.)* 39 (2009) 1362–1381.
- [40] Y. Shi, R.C. Eberhart, Fuzzy adaptive particle swarm optimization, in: *Proceedings of the 2001 Congress on Evolutionary Computation*, 2001, IEEE, 2001, pp. 101–106.

- [41] X. Hu, R.C. Eberhart, Adaptive particle swarm optimization: detection and response to dynamic systems, in: *Proceedings of the 2002 Congress on Evolutionary Computation*, 2002. CEC'02, IEEE, 2002, pp. 1666–1670.
- [42] T. Krink, M. Løvbjerg, The lifecycle model: combining particle swarm optimisation, genetic algorithms and hillclimbers, in: *International Conference on Parallel Problem Solving from Nature*, Springer, 2002, pp. 621–630.
- [43] T. Hendtlass, A combined swarm differential evolution algorithm for optimization problems, in: *International Conference on Industrial, Engineering and Other Applications of Applied Intelligent Systems*, Springer, 2001, pp. 11–18.
- [44] J. Fang, G. Sun, N. Qiu, G.P. Steven, Q. Li, Topology optimization of multicell tubes under out-of-plane crushing using a modified artificial bee colony algorithm, *J. Mech. Des.* 139 (2017) 071403.
- [45] A. Alavi Nia, M. Parsapour, Comparative analysis of energy absorption capacity of simple and multi-cell thin-walled tubes with triangular, square, hexagonal and octagonal sections, *Thin-Walled Struct.* 74 (2014) 155–165.
- [46] J.O. Hallquist, LS-DYNA theory manual, 3, Livermore Software Technology corporation, 2006.
- [47] T. Belytschko, J.I. Lin, T. Chen-Shyh, Explicit algorithms for the nonlinear dynamics of shells, *Comput. Methods Appl. Mech. Eng.* 42 (1984) 225–251.
- [48] R. Mohammadi, S.M.T.F. Ghomi, F. Jolai, Prepositioning emergency earthquake response supplies: a new multi-objective particle swarm optimization algorithm, *Appl. Math. Model.* 40 (2016) 5183–5199.
- [49] I. Lou, Z. Xie, W.K. Ung, K.M. Mok, Integrating support vector regression with particle swarm optimization for numerical modeling for algal blooms of freshwater, *Appl. Math. Model.* 39 (2015) 5907–5916.
- [50] O.E. Turgut, Hybrid chaotic quantum behaved particle swarm optimization algorithm for thermal design of plate fin heat exchangers, *Appl. Math. Model.* 40 (2016) 50–69.
- [51] A.O.S. Moraes, J.F. Mitre, P.L.C. Lage, A.R. Secchi, A robust parallel algorithm of the particle swarm optimization method for large dimensional engineering problems, *Appl. Math. Model.* 39 (2015) 4223–4241.
- [52] Ş. Gülcü, H. Kodaz, A novel parallel multi-swarm algorithm based on comprehensive learning particle swarm optimization, *Eng. Appl. Artif. Intell.* 45 (2015) 33–45.
- [53] B. Li, D. Li, Z. Zhang, S. Yang, F. Wang, Slope stability analysis based on quantum-behaved particle swarm optimization and least squares support vector machine, *Appl. Math. Model.* 39 (2015) 5253–5264.
- [54] M.A. Khanesar, M. Teshnehlab, M.A. Shoorehdeli, A novel binary particle swarm optimization, in: *Mediterranean Conference on Control & Automation*, 2007. MED'07, IEEE, 2007, pp. 1–6.
- [55] N. Jin, Y. Rahmat-Samii, Advances in particle swarm optimization for antenna designs: Real-number, binary, single-objective and multiobjective implementations, *IEEE Trans. Antennas Propag.* 55 (2007) 556–567.
- [56] T. Zegard, G.H. Paulino, Bridging topology optimization and additive manufacturing, *Struct. Multidiscip. Optim.* 53 (2015) 175–192.
- [57] D. Zeng, F. Duddeck, Improved hybrid cellular automata for crashworthiness optimization of thin-walled structures, *Struct. Multidiscip. Optim.* 56 (2017) 101–115.